PERGAMON

International Journal of Multiphase Flow 27 (2001) 1011–1028

International Journal of Multiphase Flow

www.elsevier.com/locate/ijmulflow

Onsets of entrainment during dual discharge from a stratified two-phase region through horizontal branches with centrelines falling in an inclined plane: Part 1 – Analysis of liquid entrainment

M.R. Maier, H.M. Soliman *, G.E. Sims, K.F. Armstrong

Department of Mechanical and Industrial Engineering, University of Manitoba, Winnipeg, Manitoba, Canada R3T 5V6

Received 3 August 1999; received in revised form 1 October 2000

Abstract

A theoretical investigation has been conducted for predicting the critical liquid height and the location of liquid entrainment during dual discharge from a stratified two-phase region through branches mounted on a vertical wall. The two branches are horizontal and their centrelines fall in a common inclined plane. Two models have been developed; a simplified point-sink model and a more-accurate finite-branch model. Predictions from the two models are shown to be in good agreement for the condition of high flow rates from the branches, while the finite-branch model is necessary for good predictions at low branch flow rates. Influences of the various independent parameters on the predicted onset are presented and discussed. Comparisons with experimental results are shown in Part 2 of this paper.

Keywords: Theoretical analysis; Dual discharge; Liquid entrainment; Branches falling in an inclined plane

1. Introduction

Several applications involve two-phase discharge from large pipes or manifolds through single and multiple branches. Examples of these applications include the flow through small breaks in the cooling channels of nuclear reactors during loss-of-coolant accidents, two-phase distribution systems where a certain incoming stream fed into a large header is divided among a number of discharging streams, and multi-passage shell-and-tube heat exchangers. Knowledge of the flow

* Corresponding author. Tel.: +1-204-474-9307; fax: +1-204-275-7507.
E-mail address: hsolima@cc.umanitoba.ca (H.M. Soliman).

0301-9322/01/$ - see front matter
PII: S0301-9322(00)00059-8

phenomena involved in these applications is obviously essential for the design and performance prediction of such devices.

For a single discharge from a large channel containing stratified two-phase flow, Zuber (1980) pointed out that two distinct phenomena may occur depending on the location of the branch relative to the gas–liquid interface. If the branch is below the interface, gas can be entrained into the predominantly liquid flow through the branch. On the other hand, if the branch is located above the interface, liquid may be entrained into the predominantly gas flow through the branch. Knowledge of the conditions at the onsets of gas and liquid entrainment is obviously very important because these phenomena influence the mass flow rate and quality in the branch. Theoretical and experimental investigations were reported for determining the onsets of entrainment under different flow configurations. The experimental studies are discussed in Part 2 of this paper, while the focus here is on the theoretical work.

Craya (1949) developed theoretical models for the onset of liquid entrainment during discharge from a large stratified region through a single side slot or a single side branch. He treated the slot and the branch as a line sink or as a point sink, respectively. Soliman and Sims (1991) pointed out that Craya's solution for a single side slot does not reach the appropriate limits as the discharge flow rate approaches zero and, therefore, the accuracy of Craya's result is doubtful at low discharge flow rates. A new model was developed by Soliman and Sims (1991) that took into account the finite size of the slot. The same authors (Soliman and Sims, 1992) developed a model for the onset of liquid entrainment in circular branches of finite size and demonstrated by comparison with experimental data that their model provided much better accuracy than Craya's point-sink model for low discharge flow rates.

For the case of dual discharge, Armstrong et al. (1992a) developed a model for predicting the onset of liquid entrainment in a system with two parallel slots. The slots were simulated as two-dimensional line sinks. As well, Armstrong et al. (1992b) considered the problem of dual discharge from horizontal, circular branches mounted on a vertical wall with centrelines of the branches falling in a common vertical plane. For this geometry, Armstrong et al. (1992b) developed a theoretical model (treating the branches as point sinks) and experimental data for the onset of liquid entrainment with excellent agreement between data and theory. More recently, Hassan (1995) obtained experimental data for the same geometry at low discharge flow rates and demonstrated that the point-sink analysis of Armstrong et al. (1992b) is not capable of good predictions at these conditions.

The long-term objective of our research program is to develop clear understanding of two-phase flow in multi-branch distribution headers and multi-passage heat exchangers. In these systems, the outlet branches can be located at various positions relative to each other. Keeping in mind that the current state of knowledge is complete only for the case of a single branch, a logical first step towards our long-term objective is to solve the case of two branches for the whole range of independent parameters (separating distance between the branches, angular location of one branch relative to the other, and flow rates through the branches). Therefore, the objective of the present investigation is to develop theoretical models for the onset of liquid entrainment during discharge from a stratified region through two horizontal branches mounted on a vertical wall with the centrelines of the branches falling in a common inclined plane. These models should be valid for the whole range of independent parameters. Both, point-sink and finite-branch analyses will be used. Experimental data on gas and liquid entrainment for the two-branch geometry, as

well as comparisons with the present theory, are presented in Part 2 of this paper in order to validate the methodology used in the theoretical part.

2. Theoretical analysis

The configuration for the present analysis is shown in Fig. 1. A stratified layer of two immiscible fluids (representing the gas and the liquid) of densities ρ and $(\rho + \Delta\rho)$ is contained in a large reservoir. Two horizontal branches are mounted on the plane vertical wall of the reservoir separated by a distance L (centre-to-centre) and the plane passing through the branch centrelines is inclined at an angle α from the horizontal x-axis. The branches are assumed to have a square $(d \times d)$ cross-section for mathematical convenience. However, as shown later, the results for the square cross-section are very close to those of a circular branch. Discharge is induced from the lighter fluid through the lower and upper branches with mass flow rates of $\dot{m}_1$ and $\dot{m}_2$, respectively. There is a critical height h (measured from the centreline of the lower branch) at which the heavier fluid starts flowing into one of the two branches. This phenomenon, called the onset of liquid entrainment, may occur at branch 1, branch 2, or simultaneously at both branches, depending on $\dot{m}_1$, $\dot{m}_2$, and α. The purpose of this analysis is to predict h and the branch at which the phenomenon occurs.

The analysis assumes steady flow and that both fluids are incompressible with constant properties. Viscosity and surface-tension effects are neglected while gravity and inertia forces are dominant; therefore, potential flow is assumed throughout the flow field. The solution method follows Craya's (1949) approach, applied successfully by Armstrong et al. (1992b), consisting of three steps as follows:

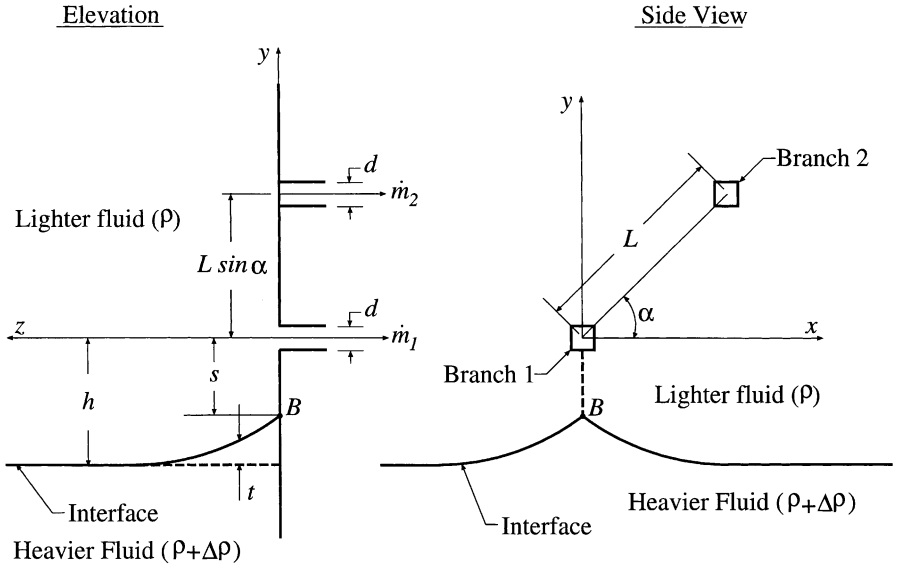

Fig. 1. Coordinate system and relevant parameters for finite-branch analysis.

(a) Determine the equilibrium condition of the interface.
(b) Determine the velocity field in the lighter fluid.
(c) Impose equality of the velocity and its gradient at linking point B (shown in Fig. 1) as the criteria for the onset.

There are two alternatives in executing step (b) above. One alternative is to treat the branches as point sinks (see Fig. 2), which simplifies the analysis and leads to a simple algebraic formulation for the critical height. The second alternative is to take into consideration the finite size of the branches (as shown in Fig. 1) with the expected consequence of a more complex (but closed form) result. Previous results for a single branch (Soliman and Sims, 1992) have shown that for low branch flow rates, the point-sink analysis does not provide good accuracy and the finite-branch analysis is necessary. However, for moderate and high branch flow rates, the two analyses were found to agree closely. In the present work, results will be obtained using both, the point-sink and finite-branch analyses.

2.1. Equilibrium of the interface

The equilibrium at the interface is controlled by a balance between gravity and inertia forces. Applying Bernoulli equation along a streamline coincident with the interface from the side of the lighter (moving) fluid, we get

$$P + \frac{\rho V^2}{2} + \rho g t = C, \tag{1}$$

where P is the static pressure, V the velocity, g the gravitational acceleration, t the deflection of the interface (shown in Figs. 1 and 2), and C is an arbitrary constant. Along the same streamline from the side of the heavier (stationary) fluid, Bernoulli equation gives

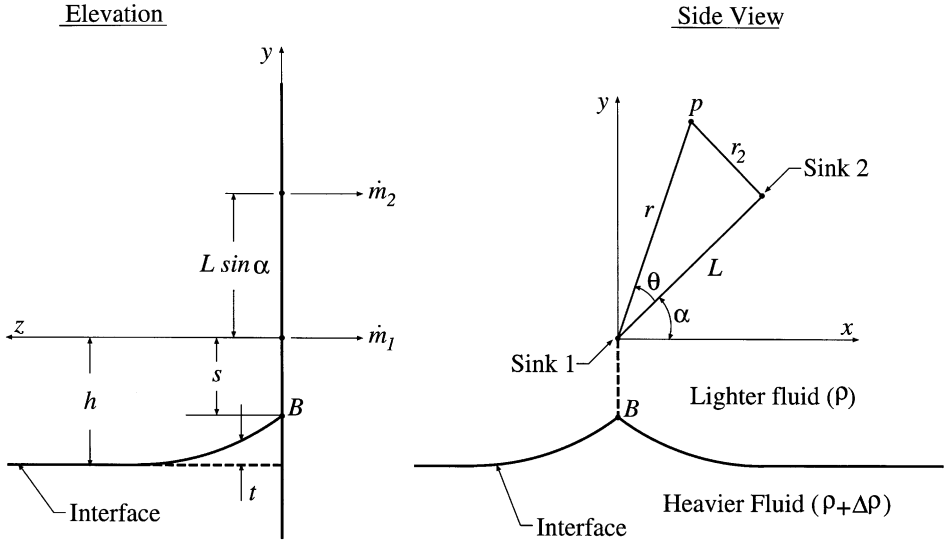

Fig. 2. Coordinate system and relevant parameters for point-sink analysis.

$$P + (\rho + \Delta\rho)gt = C. \tag{2}$$

Subtracting Eq. (2) from Eq. (1), we get

$$\frac{V^2}{2} = \frac{\Delta\rho}{\rho} gt. \tag{3}$$

Linking point B (shown in Figs. 1 and 2) corresponds to the location $t = h - s$, where h is the critical height measured from the centreline of branch 1 and s is the vertical distance between linking point B and the centreline of branch 1. Therefore, the velocity at linking point B can be obtained from

$$\frac{V_B^2}{2} = \frac{\Delta\rho}{\rho} g(h - s). \tag{4}$$

Eqs. (1)–(4) apply to both the point-sink and finite-branch analyses.

2.2. Velocity field in the lighter fluid (point-sink analysis)

With reference to Fig. 2, the two branches are simulated as point sinks with strengths n_1 and n_2, where the strength n and the mass flow rate $\dot{m}$ are related by

$$n = \frac{\dot{m}}{2\pi\rho}. \tag{5}$$

In developing the velocity field in the lighter fluid, the presence of the heavier (stationary) fluid is ignored. Therefore, the flow field is treated as a semi-infinite medium extending over $-\infty < x < \infty$, $-\infty < y < \infty$, and $0 \leqslant z < \infty$. The three-dimensional flow is symmetric around a plane that contains the two point sinks and the z-axis. Therefore, some analogy exists with the case of two-dimensional flow, thereby allowing the introduction of a stream function and a velocity potential. Following Milne-Thomson (1968), the potential function ϕ is given by

$$\phi = -\frac{n_1}{r} - \frac{n_2}{r_2}, \tag{6}$$

where r and r_2 are the radial distances from sinks 1 and 2, respectively, as shown in Fig. 2. Expressing r_2 in terms of other parameters, we get

$$\phi = -\frac{n_1}{r} - \frac{n_2}{\sqrt{r^2 + L^2 - 2rL\cos\theta}}, \tag{7}$$

where θ is an angle measured from the plane of symmetry, as shown in Fig. 2. The radial velocity V_r at any point in the flow domain can be obtained as

$$V_r = -\frac{\partial\phi}{\partial r} = -\frac{n_1}{r^2} - \frac{n_2(r - L\cos\theta)}{(r^2 + L^2 - 2rL\cos\theta)^{3/2}}. \tag{8}$$

Linking point B corresponds to the location, where $\theta = (3\pi/2 - \alpha)$ and $r = s$. Thus,

$$\frac{V_B^2}{2} = \frac{1}{2}\left[\frac{n_1}{s^2} + \frac{n_2(s + L\sin\alpha)}{(s^2 + L^2 + 2sL\sin\alpha)^{3/2}}\right]^2. \tag{9}$$

2.3. The critical height (point-sink analysis)

There are two issues to consider: (a) the sink at which the onset of entrainment would occur, and (b) the critical height h corresponding to this onset. As illustrated in Fig. 3, we will first assume that the onset of entrainment occurs at sink 1 and calculate the appropriate h_1, then repeat the process at sink 2 and calculate h_2. It should be noted from Fig. 3 that both h_1 and h_2 are measured from sink 1. Therefore, by comparing h_1 and h_2, the location of the onset of entrainment and the critical height for the system h can be determined. If $h_1 > h_2$, then the onset occurs at sink 1 and $h = h_1$. For $h_2 > h_1$, the onset occurs at sink 2 and $h = h_2$.

For determining the critical heights (h_1 and h_2), we followed the procedure applied successfully by Armstrong et al. (1992b). For fixed values of $\rho, \Delta\rho, g, \alpha, L, n_1$, and n_2, Eq. (9) provides a specific relation between $V_B^2/2$ and s represented by a single curve, while Eq. (4) produces a set of parallel straight lines whose locations depend on the value of h. For large values of h, the straight line and the curve do not intersect, while two points of intersection are possible with small values of h. There is one value of h that corresponds to a single intersection with the straight line given by Eq. (4) forming a tangent to the curve given by Eq. (9). The hypothesis here is that this value of h is the critical value for the onset. By equating the values of $V_B^2/2$ and their first derivatives with respect to s, we get (after reduction) the following non-dimensional relations for the onset of entrainment at sink 1:

$$32 = \left[A_1 Fr_1^* + A_2 Fr_2^*\right]\left[A_3 Fr_1^* + A_4 Fr_2^*\right], \tag{10}$$

and

$$H_1 = S_1 + \frac{1}{4}\left[\frac{A_1 Fr_1^* + A_2 Fr_2^*}{A_3 Fr_1^* + A_4 Fr_2^*}\right], \tag{11}$$

where Fr^* is the modified Froude number given by

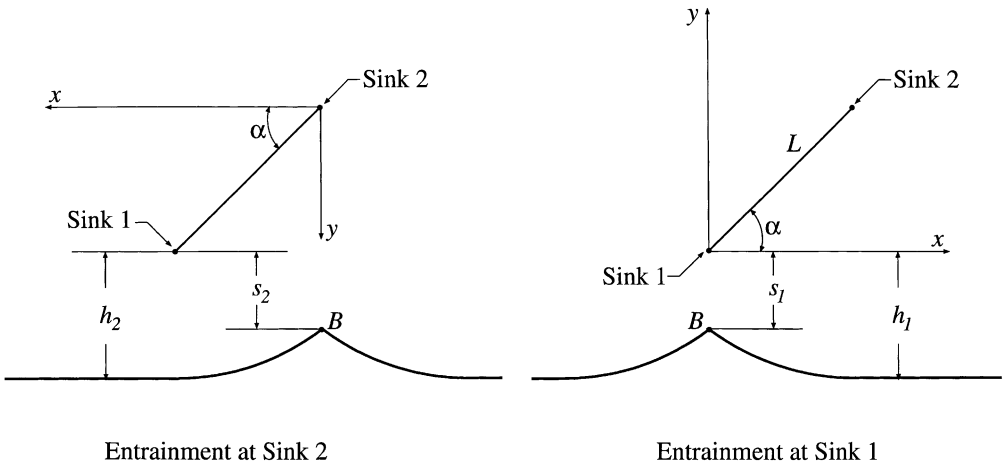

Fig. 3. Coordinate system and relevant parameters for entrainment at both sinks.

$$Fr^* = \frac{(4/\pi)\dot{m}}{\sqrt{g\rho L^5 \Delta\rho}}, \tag{12a}$$

$$S_1 = s_1/L, \tag{12b}$$

$$H_1 = h_1/L, \tag{12c}$$

$$A_1 = 1/S_1^2, \tag{12d}$$

$$A_2 = (S_1 + \sin\alpha)/\left[(S_1 + \sin\alpha)^2 + cos^2\alpha\right]^{3/2}, \tag{12e}$$

$$A_3 = 1/S_1^3, \tag{12f}$$

and

$$A_4 = \left[(S_1 + \sin\alpha)^2 - \frac{1}{2}\cos^2\alpha\right] \Big/ \left[(S_1 + \sin\alpha)^2 + \cos^2\alpha\right]^{5/2}. \tag{12g}$$

The critical height for the onset of entrainment at sink 2 could be derived using the same technique as for sink 1 following the situation described in Fig. 3, resulting in

$$32 = \left[B_1 Fr_2^* + B_2 Fr_1^*\right]\left[B_3 Fr_2^* + B_4 Fr_1^*\right], \tag{13}$$

and

$$H_2 + \sin\alpha = S_2 + \frac{1}{4}\left[\frac{B_1 Fr_2^* + B_2 Fr_1^*}{B_3 Fr_2^* + B_4 Fr_1^*}\right], \tag{14}$$

where

$$S_2 = s_2/L, \tag{15a}$$

$$H_2 = h_2/L, \tag{15b}$$

$$B_1 = 1/S_2^2, \tag{15c}$$

$$B_2 = (S_2 - \sin\alpha)/[(S_2 - \sin\alpha)^2 + \cos^2\alpha]^{3/2}, \tag{15d}$$

$$B_3 = 1/S_2^3, \tag{15e}$$

and

$$B_4 = \left[(S_2 - \sin\alpha)^2 - \frac{1}{2}\cos^2\alpha\right] \Big/ \left[(S_2 - \sin\alpha)^2 + \cos^2\alpha\right]^{5/2}. \tag{15f}$$

For given values of $\dot{m}_1, \dot{m}_2, \rho, \Delta\rho, L$, and α, the values of Fr_1^* and Fr_2^* can be obtained from Eq. (12a), the corresponding values of S_1 and S_2 can be obtained from Eqs. (10) and (13), respectively, and the values of H_1 and H_2 can be obtained from Eqs. (11) and (14), respectively. By comparing H_1 and H_2, the value of $H = h/L$ can be determined as explained earlier. The form of Eqs. (10), (11), (12a)–(12g), (13), (14), (15a)–(15f) suggests that H is dependent only on Fr_1^*, Fr_2^* and α for all values of L.

For the special case of a single discharge (i.e., $Fr_2^* = 0$), Eqs. (10) and (11) produce $H_1 = 0.625(Fr_1^*)^{0.4}$, which is consistent with previous results (Craya, 1949). For $\alpha = 0$, Eqs. (10),

(11), (12a)–(12g) for sink 1 are identical to Eqs. (13), (14), (15a)–(15f) for sink 2, as expected from symmetry.

We note that for the limiting case $Fr_1^* = Fr_2^* = 0$, the above analysis converges to $H_1 = H_2 = 0$. For a branch of a finite size (circular with diameter d or square with side d), the correct limit should be $h = d/2$. Therefore, the accuracy of the point-sink analysis may be questionable at low discharges. In the following section, a more elaborate analysis is presented for improved accuracy at low values of Fr_1^* and Fr_2^*. This analysis is based on all the simplifying assumptions used in the previous point-sink analysis, except for the adoption of finite branch sizes.

2.4. The finite-branch analysis

Ignoring the presence of the heavier fluid and referring to Fig. 1, the flow field in the lighter fluid extends over the semi-infinite region defined by $-\infty < x < \infty, -\infty < y < \infty$, and $0 \leqslant z < \infty$. The flow is caused by two discharges with uniform velocities; V_{d1} from branch 1 situated at $-d/2 \leqslant x \leqslant d/2, -d/2 \leqslant y \leqslant d/2$, and $z = 0$, and V_{d2} from the upper branch situated at $(L\cos\alpha - d/2) \leqslant x \leqslant (L\cos\alpha + d/2)$, $(L\sin\alpha - d/2) \leqslant y \leqslant (L\sin\alpha + d/2)$, and $z = 0$. With the assumptions stated above, the velocity field is obtained from the continuity equation,

$$\frac{\partial V_x}{\partial x} + \frac{\partial V_y}{\partial y} + \frac{\partial V_z}{\partial z} = 0, \tag{16}$$

where V_x, V_y, and V_z are the velocity components in the x, y, and z directions. Introducing a scalar potential function ϕ, such that

$$V_x = \frac{\partial \phi}{\partial x}, V_y = \frac{\partial \phi}{\partial y}, \text{ and } V_z = \frac{\partial \phi}{\partial z}, \tag{17}$$

we get the well-known Laplace equation

$$\frac{\partial^2 \phi}{\partial x^2} + \frac{\partial^2 \phi}{\partial y^2} + \frac{\partial^2 \phi}{\partial z^2} = 0. \tag{18}$$

Eq. (18) is subject to the following boundary conditions:

$$\begin{aligned} &\text{at } z = 0, \\ &\frac{\partial \phi}{\partial z} = -V_{d1}, -d/2 \leqslant x \leqslant d/2 \quad \text{and} -d/2 \leqslant y \leqslant d/2 \\ &\qquad = -V_{d2}, (L\cos\alpha - d/2) \leqslant x \leqslant (L\cos\alpha + d/2) \\ &\qquad\quad \text{and } (L\sin\alpha - d/2) \leqslant y \leqslant (L\sin\alpha + d/2) \\ &\qquad = 0 \text{ at all other values of } x \text{ and } y \end{aligned} \tag{19}$$

$$\text{as } x \to \pm\infty, y \to \pm\infty, \text{ or } z \to \infty, \phi \text{ is finite.} \tag{20}$$

A solution of Eq. (18) satisfying boundary conditions (19) and (20) was obtained using the method of separation of variables. Details of the derivation are available in Maier (1998). A new expression for $V_B^2/2$ was derived from the three-dimensional velocity profile. By equating the values of $V_B^2/2$ from this expression and Eq. (4), as well as their first derivatives with respect to s,

the following non-dimensional relations were obtained for determining the critical height h_1 for the onset of entrainment at branch 1:

$$32(d/L)^5 = [C_1 Fr_1^* + C_2 Fr_2^*][C_3 Fr_1^* + C_4 Fr_2^*], \tag{21}$$

and

$$H_1 = S_1 + \frac{1}{4}\left(\frac{d}{L}\right)\left[\frac{C_1 Fr_1^* + C_2 Fr_2^*}{C_3 Fr_1^* + C_4 Fr_2^*}\right], \tag{22}$$

where,

$$C_1 = \frac{{}_2F_1(0.5, 0.5, 1.5; -0.25E_1^{-2})}{E_1} - \frac{{}_2F_1(0.5, 0.5, 1.5; -0.25E_2^{-2})}{E_2}, \tag{23a}$$

$$C_2 = E_6\left[\frac{{}_2F_1(0.5, 0.5, 1.5; -E_6^2E_3^{-2})}{E_3} - \frac{{}_2F_1(0.5, 0.5, 1.5; -E_6^2E_4^{-2})}{E_4}\right] + E_5\left[\frac{{}_2F_1(0.5, 0.5, 1.5; -E_5^2E_4^{-2})}{E_4} - \frac{{}_2F_1(0.5, 0.5, 1.5; -E_5^2E_3^{-2})}{E_3}\right], \tag{23b}$$

$$C_3 = \frac{1}{24}\left[\frac{{}_2F_1(1.5, 1.5, 2.5; -0.25E_2^{-2})}{E_2^4} - \frac{{}_2F_1(1.5, 1.5, 2.5; -0.25E_1^{-2})}{E_1^4}\right] - \frac{1}{2}\left[\frac{{}_2F_1(0.5, 0.5, 1.5; -0.25E_2^{-2})}{E_2^2} - \frac{{}_2F_1(0.5, 0.5, 1.5; -0.25E_1^{-2})}{E_1^2}\right], \tag{23c}$$

$$C_4 = \frac{1}{6}\left[E_6^3\left\{\frac{{}_2F_1(1.5, 1.5, 2.5; -E_6^2E_4^{-2})}{E_4^4} - \frac{{}_2F_1(1.5, 1.5, 2.5; -E_6^2E_3^{-2})}{E_3^4}\right\} + E_5^3\left\{\frac{{}_2F_1(1.5, 1.5, 2.5; -E_5^2E_3^{-2})}{E_3^4} - \frac{{}_2F_1(1.5, 1.5, 2.5; -E_5^2E_4^{-2})}{E_4^4}\right\}\right] - \frac{1}{2}\left[E_6\left\{\frac{{}_2F_1(0.5, 0.5, 1.5; -E_6^2E_4^{-2})}{E_4^2} - \frac{{}_2F_1(0.5, 0.5, 1.5; -E_6^2E_3^{-2})}{E_3^2}\right\} + E_5\left\{\frac{{}_2F_1(0.5, 0.5, 1.5; -E_5^2E_3^{-2})}{E_3^2} - \frac{{}_2F_1(0.5, 0.5, 1.5; -E_5^2E_4^{-2})}{E_4^2}\right\}\right] \tag{23d}$$

$$E_1 = S_1(L/d) - 0.5, \tag{23e}$$

$$E_2 = E_1 + 1, \tag{23f}$$

$$E_3 = (S_1 + \sin\alpha)(L/d) - 0.5, \tag{23g}$$

$$E_4 = E_3 + 1, \tag{23h}$$

$$E_5 = (L/d)\cos\alpha - 0.5, \tag{23i}$$

and

$$E_6 = E_5 + 1. \tag{23j}$$

Eqs. (21) and (22) have the same form as Eqs. (10) and (11), but with different coefficients. The function ${}_2F_1\ (a, b, c; w)$ appearing in Eqs. (23a)–(23j) is the complex hypergeometric function of the variable w with parameters $a, b,$ and c. The procedure outlined by Press et al. (1992) for evaluating this function was followed in the present computations.

The critical height for the onset of entrainment at branch 2 could be derived using the same technique as for branch 1. The result can be placed in the following form:

$$32(d/L)^5 = [D_1 Fr_2^* + D_2 Fr_1^*][D_3 Fr_2^* + D_4 Fr_1^*], \tag{24}$$

and

$$H_2 + \sin\alpha = S_2 + \frac{1}{4}\left(\frac{d}{L}\right)\left[\frac{D_1 Fr_2^* + D_2 Fr_1^*}{D_3 Fr_2^* + D_4 Fr_1^*}\right], \tag{25}$$

where,

$$D_1 = \frac{{}_2F_1(0.5, 0.5, 1.5; -0.25G_1^{-2})}{G_1} - \frac{{}_2F_1(0.5, 0.5, 1.5; -0.25G_2^{-2})}{G_2}, \tag{26a}$$

$$D_2 = G_6\left[\frac{{}_2F_1(0.5, 0.5, 1.5; -G_6^2G_3^{-2})}{G_3} - \frac{{}_2F_1(0.5, 0.5, 1.5; -G_6^2G_4^{-2})}{G_4}\right] + G_5\left[\frac{{}_2F_1(0.5, 0.5, 1.5; -G_5^2G_4^{-2})}{G_4} - \frac{{}_2F_1(0.5, 0.5, 1.5; -G_5^2G_3^{-2})}{G_3}\right], \tag{26b}$$

$$D_3 = \frac{1}{24}\left[\frac{{}_2F_1(1.5, 1.5, 2.5; -0.25G_2^{-2})}{G_2^4} - \frac{{}_2F_1(1.5, 1.5, 2.5; -0.25G_1^{-2})}{G_1^4}\right] - \frac{1}{2}\left[\frac{{}_2F_1(0.5, 0.5, 1.5; -0.25G_2^{-2})}{G_2^2} - \frac{{}_2F_1(0.5, 0.5, 1.5; -0.25G_1^{-2})}{G_1^2}\right], \tag{26c}$$

$$D_4 = \frac{1}{6}\left[G_6^3\left\{\frac{{}_2F_1(1.5, 1.5, 2.5; -G_6^2G_4^{-2})}{G_4^4} - \frac{{}_2F_1(1.5, 1.5, 2.5; -G_6^2G_4^{-2})}{G_3^4}\right\} + G_5^3\left\{\frac{{}_2F_1(1.5, 1.5, 2.5; -G_5^2G_3^{-2})}{G_3^4} - \frac{{}_2F_1(1.5, 1.5, 2.5; -G_5^2G_4^{-2})}{G_4^4}\right\}\right] - \frac{1}{2}\left[G_6\left\{\frac{{}_2F_1(0.5, 0.5, 1.5; -G_6^2G_4^{-2})}{G_4^2} - \frac{{}_2F_1(1.5, 1.5, 2.5; -G_6^2G_3^{-2})}{G_3^2}\right\} + G_5\left\{\frac{{}_2F_1(0.5, 0.5, 1.5; -G_5^2G_3^{-2})}{G_3^2} - \frac{{}_2F_1(0.5, 0.5, 1.5; -G_5^2G_4^{-2})}{G_4^2}\right\}\right], \tag{26d}$$

$$G_1 = -S_2(L/d) - 0.5, \tag{26e}$$

$$G_2 = G_1 + 1, \tag{26f}$$

$$G_3 = (S_2 - \sin\alpha)(L/d) - 0.5, \tag{26g}$$

$$G_4 = G_3 + 1, \tag{26h}$$

$$G_5 = -(L/d)\cos\alpha - 0.5, \tag{26i}$$

and

$$G_6 = G_5 + 1. \tag{26j}$$

According to Eqs. (21), (22), (23a)–(23j), (24), (25), (26a)–(26j), the critical heights H_1 and H_2 are dependent on $Fr_1^*, Fr_2^*, (L/d)$, and α. For given values of these independent parameters, H_1 can be determined from Eqs. (21), (22), (23a)–(23j), H_2 can be determined from Eqs. (24), (25), (26a)–(26j), and H is selected as the larger of the two.

3. Theoretical results and discussion

In the finite-branch analysis, the branches were assumed to have a square cross-section, rather than the commonly used circular one. With this assumption, it was possible to develop a closed-form solution for the critical height at the onset. Before presenting the results of the present analysis, an assessment of the influence of this assumption will be made. Fig. 4 shows three sets of results for discharge from a single horizontal branch mounted on a vertical wall. These results correspond to the present point-sink analysis, the present finite-branch analysis, and a previous analysis by Soliman and Sims (1992) for a finite branch of a circular cross-section. All results are presented in terms of h/d versus Fr, where the Froude number Fr is given by

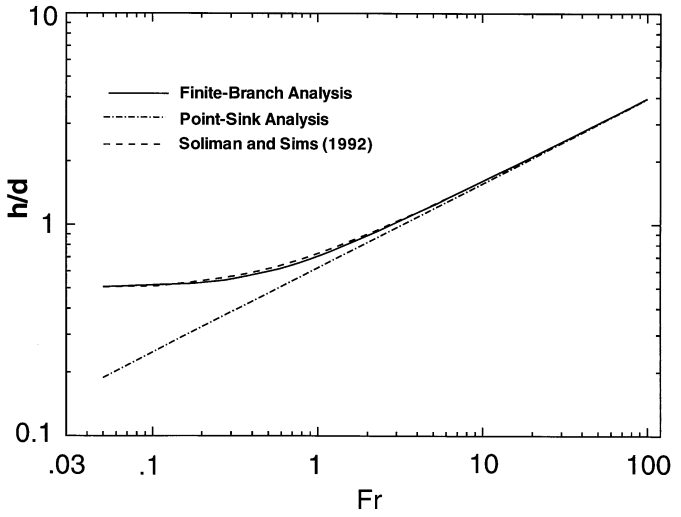

Fig. 4. Comparison among three predictions of the critical height for single discharge.

$$Fr = (L/d)^{2.5} Fr^* = \frac{(4/\pi)\dot{m}}{\sqrt{gd^5\rho\Delta\rho}}. \tag{27}$$

Fig. 4 shows that the results of the square and circular branches are practically identical for all values of Fr. Both sets of results converge to the correct limit $h/d = 0.5$ as $Fr \to 0$. The deviation between these two sets of results and the point-sink results is large at low Fr. However, for $Fr > 10$, the three sets of results are in close agreement.

According to the present finite-branch analysis, $H = H(Fr_1^*, Fr_2^*, L/d, \alpha)$. If we use Fr, rather than Fr^*, the correlation would still contain four independent variables, i.e., $H = H(Fr_1, Fr_2, L/d, \alpha)$. Since Fr is more commonly used in the literature and there is no loss in generality by using it, we decided to present all remaining results in terms of Fr, rather than Fr^*.

Fig. 5 shows a comparison between the results from the point-sink analysis and the finite branch analysis for $\alpha = 90^\circ$ and $L/d = 2$. In this case, entrainment always happens at branch 1. For low values of Fr_1 and Fr_2, large deviation can be seen in the predicted values of h/d from the two models. The deviation decreases as Fr_1 and/or Fr_2 increase. For example, this deviation is small at $Fr_1 > 10$ for all values of Fr_2, or at $Fr_2 > 45$ for all values of Fr_1. The results in Fig. 5 confirm that the more-accurate finite-branch analysis must be used for conditions of low Fr_1 and Fr_2.

A sample of the results from the finite-branch analysis is presented in Figs. 6 and 7 with $L/d = 2$ in both sets of results. In Fig. 6, corresponding to $\alpha = 30^\circ$, the behaviour of h/d is presented as a function of Fr_1 and Fr_2. For a fixed value of Fr_2 (e.g., $Fr_2 = 30$), the onset of

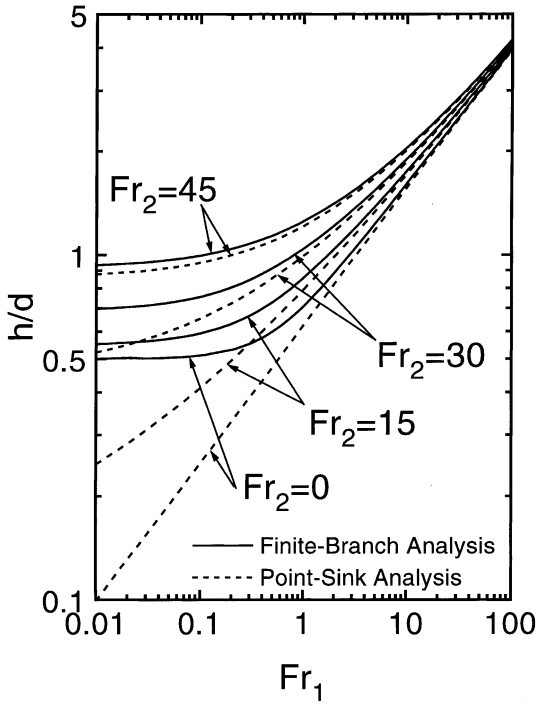

Fig. 5. Comparison between the point-sink and finite branch models for $\alpha = 90^\circ$ and $L/d = 2$.

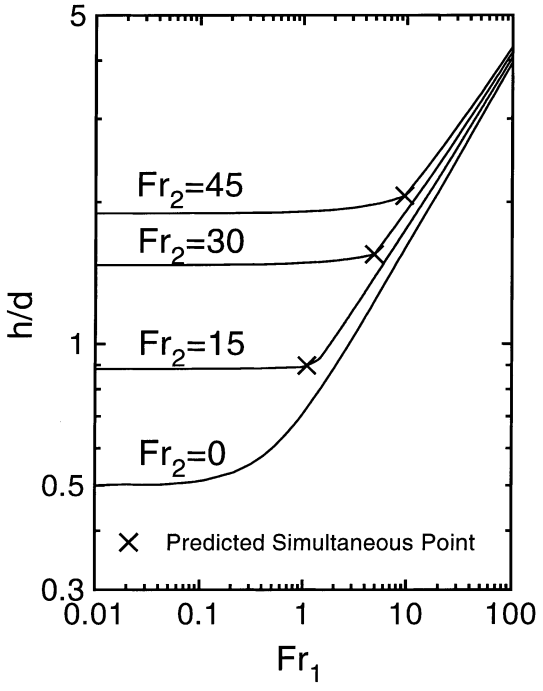

Fig. 6. Entrainment predictions for $\alpha = 30^\circ$ and $L/d = 2$.

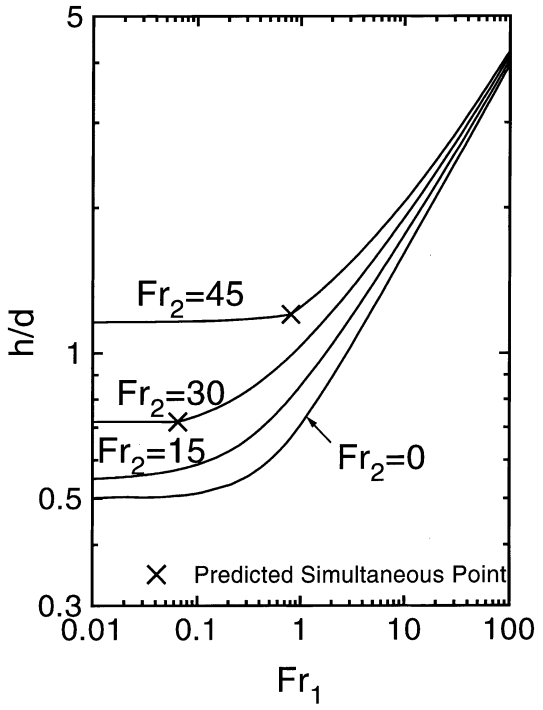

Fig. 7. Entrainment predictions for $\alpha = 60^\circ$ and $L/d = 2$.

entrainment occurs at branch 2 for low values of Fr_1. There is a gentle increase in h/d as Fr_1 increases up to the point where the onset of entrainment occurs simultaneously at both branches ($Fr_1 \approx 5$ when $Fr_2 = 30$). Beyond this point, the onset shifts to branch 1 and h/d increases significantly with Fr_1. As expected, for a fixed α, the value of Fr_1 at the point of simultaneous onsets increases as Fr_2 increases. As well, comparing the results in Figs. 6 and 7, we can see that for a fixed Fr_2, the value of Fr_1 at the point of simultaneous onsets decreases as α increases. Comparing the results in Figs. 5–7, it can be seen that values of h/d for entrainment at branch 2 drop significantly as α increases at the same values of Fr_1 and Fr_2. This trend is consistent with the fact that as α increases, the vertical distance between branch 2 and the interface increases and, therefore, h_2 (measured from centreline of branch 1, as shown in Fig. 3) decreases.

The influence of α on h/d is examined in detail in Figs. 8 and 9. It is clear from Fig. 8 (corresponding to $Fr_2 = 30$ and $L/d = 2$) that h/d decreases as α increases, particularly when the onset of entrainment occurs at branch 2. However, a reversal in trend can be seen in Fig. 9 (corresponding to $Fr_2 = 30$ and $L/d = 4$), where the values of h/d for $\alpha = 90^\circ$ exceed those for $\alpha = 40^\circ$. For both angles, the onset is taking place at branch 1. This reversal of trend raises a question about the effect of α on the velocity distribution near branch 1 for fixed values of Fr_1, Fr_2, and L/d. This question is addressed later in connection with Fig. 11.

The influence of L/d on h/d is presented in Fig. 10 for $Fr_2 = 30$ and $\alpha = 60^\circ$. These results show that h/d decreases as L/d increases for the same Fr_1, Fr_2, and α. This trend is consistent with the physics of the problem since an increase in L/d decreases the influence of branch 2, thus moving

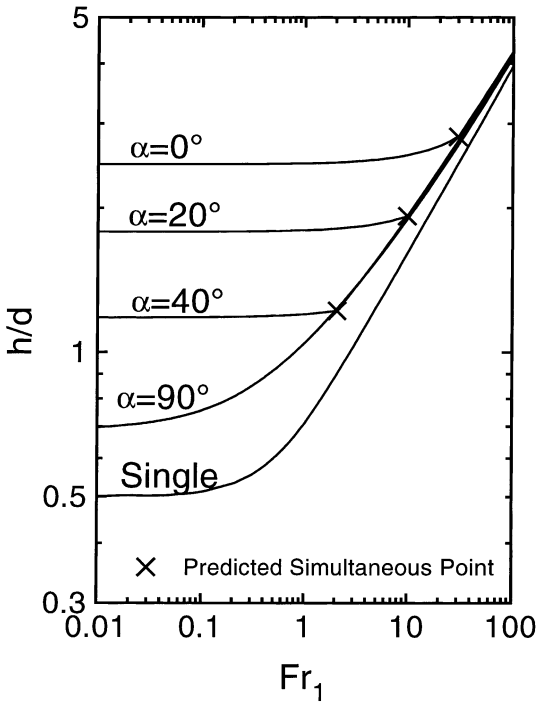

Fig. 8. Influence of α on h/d for $Fr_2 = 30$ and $L/d = 2$.

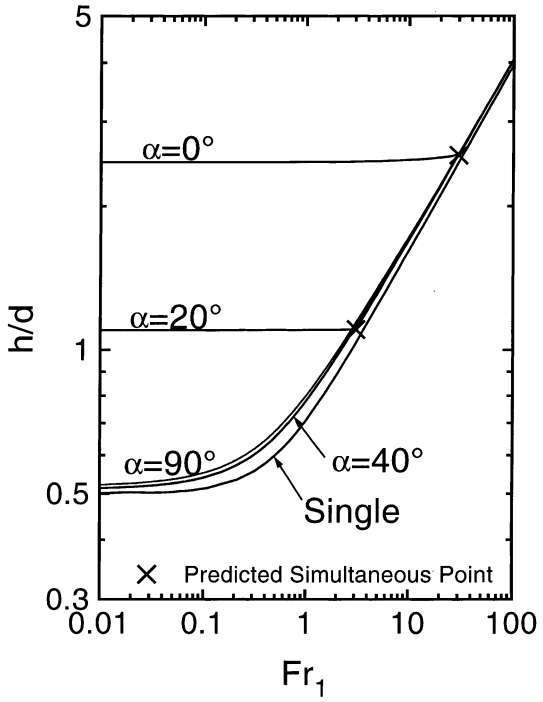

Fig. 9. Influence of α on h/d for $Fr_2 = 30$ and $L/d = 4$.

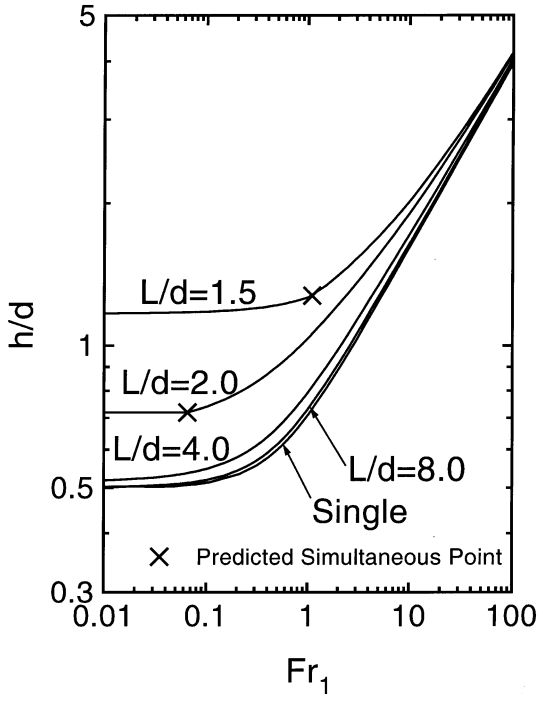

Fig. 10. Influence of L/d on h/d for $Fr_2 = 30$ and $\alpha = 60°$.

the results towards the case of single discharge. Actually, Fig. 10 shows that the single-discharge performance is closely approached at $L/d = 8$.

An interesting way of presenting the results is shown in Fig. 11, where h/d is plotted against α for various values of Fr_1 with $Fr_2 = 30$ and $L/d = 2$. This figure shows that for $Fr_1 > Fr_2$, the onset of entrainment always occurs at branch 1 and h/d decreases slightly with α. For $Fr_1 = Fr_2$, the onset of entrainment occurs simultaneously at branches 1 and 2 for $\alpha = 0$. Beyond that point, the onset of entrainment shifts to branch 1 with a slightly decreasing h/d with α. For $Fr_1 < Fr_2$, the onset of entrainment occurs first at branch 2 up to a certain value of α (where simultaneous entrainment occurs), beyond which entrainment shifts to branch 1. The value of α at the simultaneous-entrainment point increases as Fr_1 decreases. For $Fr_1 = 0$, the onset of entrainment occurs at branch 2 for all α. After the entrainment shifts to branch 1, the behaviour of h/d against α appears to depend on the value of Fr_1. For $Fr_1 \geqslant 5$, h/d decreases slightly as α increases, while for $Fr_1 = 0.1$ and 1.0, h/d appears to increase slightly with α (see Fig. 11). This reversal of trend is predicted by both, the point-sink and finite-branch analyses. In order to explore the validity of this trend, we examined the formulation of V_B given by Eq. (9),

$$V_B = \frac{n_1}{s^2} + \frac{n_2(s + L\sin\alpha)}{(s^2 + L^2 + 2sL\sin\alpha)^{3/2}}. \tag{28}$$

For fixed values of n_1 and n_2 (i.e., fixed Fr_1 and Fr_2), and also fixed values of s and L, we can determine the effect of α on V_B. The first term in the right-hand side of Eq. (28) is fixed (effect of

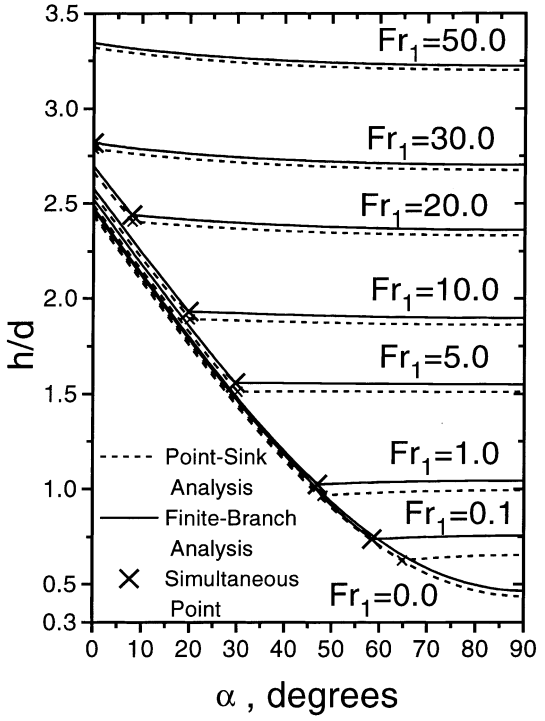

Fig. 11. Entrainment predictions from both models for $Fr_2 = 30$ and $L/d = 2$.

sink 1), while the second term (effect of sink 2) varies with α. Calculating $\partial V_B/\partial\alpha$ and equating the result to zero, we get

$$s/L = (\sqrt{8 + \sin^2\ \alpha} - \sin\alpha)/4. \tag{29}$$

At $\alpha = 30^\circ$, Eq. (29) gives $s/L = 0.593$. Upon substituting $s/L = 0.593$ in $\partial V_B/\partial\alpha$, we found $\partial V_B/\partial\alpha > 0$ for $0 \leqslant \alpha < 30^\circ$, $\partial V_B/\partial\alpha = 0$ at $\alpha = 30^\circ$ and $\partial V_B/\partial\alpha < 0$ for $30 < \alpha \leqslant 90^\circ$. These results suggest that sink 2 does not always aid sink 1 in entraining. Depending on α, sink 2 may have an aiding or opposing effect on entrainment at sink 1. This behaviour explains the reversal in trend in Figs. 9 and 11.

Experimental validation of the theoretical results presented in this paper is provided in the companion paper by Maier et al. (2001).

4. Concluding remarks

The phenomenon of the onset of liquid entrainment was investigated theoretically for the condition of simultaneous discharge from a stratified two-phase region through two horizontal branches mounted on a vertical wall with the centrelines of the branches falling in an inclined plane with an angle α from the horizontal. Two models (a point-sink model and a finite-branch model) were developed for predicting the location of the onset (branch 1 or 2) and the critical height at the onset. Predictions from the two models are shown to be in good agreement for conditions of high Fr_1 and/or high Fr_2. However, when both Fr_1 and Fr_2 are low, the point-sink model does not provide accurate predictions, and the application of the finite-branch model is recommended for these conditions.

Effects of the four independent parameters $Fr_1, Fr_2, L/d$, and α on h/d were investigated. It is shown that h/d increases as Fr_1 or Fr_2 increases, however, for given values of L/d and α, the location of the onset depends on the relative values of Fr_1 and Fr_2. The effect of L/d is monotonic with h/d decreasing with an increase in L/d. At L/d of about 8, the results approach the case of a single discharge. An interesting behaviour was found while examining the effect of α at fixed Fr_1, Fr_2, and L/d. It is shown that if the onset occurs at branch 1, h/d may increase or decrease with increasing α. An explanation is provided for this mixed trend.

Acknowledgements

The financial support provided by the Natural Sciences and Engineering Research Council of Canada is gratefully acknowledged.

References

Armstrong, K.F., Soliman, H.M., Sims, G.E., Richards, J.J., 1992a. The onset of liquid entrainment for a system with two parallel slots. International Communications in Heat and Mass Transfer 19, 827–839.

Armstrong, K.F., Parrott, S.D., Sims, G.E., Soliman, H.M., Krishnan, V.S., 1992b. Theoretical and experimental study of the onset of liquid entrainment during dual discharge from large reservoirs. International Journal of Multiphase Flow 18, 217–227.

Craya, A., 1949. Theoretical research on the flow of non-homogeneous fluids. La Houille Blanche 4, 44–55.

Hassan, I.G., 1995. Single, dual and triple discharge from a large, stratified, two-phase region through small branches. Ph.D. thesis, University of Manitoba.

Maier, M.R., 1998. Onsets of liquid and gas entrainment during discharge from a stratified air–water region through two horizontal side branches with centrelines falling in an inclined plane. M.Sc. thesis, University of Manitoba.

Maier, M.R., Soliman, H.M., Sims, G.E., 2001. Onsets of entrainment during dual discharge from a stratified two-phase region through horizontal branches with centrelines falling in an inclined plane: Part 2 Experiments on gas and liquid entrainment. International Journal of Multiphase Flow 27, 1029–1049.

Milne-Thomson, L.M., 1968. Theoretical Hydrodynamics, fifth ed. MacMillan, London, UK.

Press, W.H., Teukolsky, S.A., Vetterling, W.T., Flannery, B.P., 1992. Numerical Recipes in FORTRAN, The Art of Scientific Computing, second ed. Cambridge University Press, Cambridge, UK.

Soliman, H.M., Sims, G.E., 1991. Theoretical analysis of the onset of liquid entrainment for slots of finite width. International Journal of Heat and Fluid Flow 12, 360–364.

Soliman, H.M., Sims, G.E., 1992. Theoretical analysis of the onset of liquid entrainment for orifices of finite diameter. International Journal of Multiphase Flow 18, 229–235.

Zuber, N., 1980. Problems in modelling of small break LOCA. Nuclear Regulatory Commission Report, NUREG-0724.